Structural basis of the relaxed state of a Ca^{2+}-regulated myosin filament and its evolutionary implications

John L. Woodhead, Fa-Qing Zhao, and Roger Craig[1]

Department of Cell and Developmental Biology, University of Massachusetts Medical School, Worcester, MA 01655

Edited by Hugh E. Huxley, Rosenstiel Basic Medical Sciences Research Center, Waltham, MA, and approved April 3, 2013 (received for review October 22, 2012)

Myosin filaments of muscle are regulated either by phosphorylation of their regulatory light chains or Ca^{2+} binding to the essential light chains, contributing to on–off switching or modulation of contraction. Phosphorylation-regulated filaments in the relaxed state are characterized by an asymmetric interaction between the two myosin heads, inhibiting their actin binding or ATPase activity. Here, we have tested whether a similar interaction switches off activity in myosin filaments regulated by Ca^{2+} binding. Cryo-electron microscopy and single-particle image reconstruction of Ca^{2+}-regulated (scallop) filaments reveals a helical array of myosin head-pair motifs above the filament surface. Docking of atomic models of scallop myosin head domains into the motifs reveals that the heads interact in a similar way to those in phosphorylation-regulated filaments. The results imply that the two major evolutionary branches of myosin regulation—involving phosphorylation or Ca^{2+} binding—share a common structural mechanism for switching off thick-filament activity in relaxed muscle. We suggest that the Ca^{2+}-binding mechanism evolved from the more ancient phosphorylation-based system to enable rapid response of myosin-regulated muscles to activation. Although the motifs are similar in both systems, the scallop structure is more tilted and higher above the filament backbone, leading to different intermolecular interactions. The reconstruction reveals how the myosin tail emerges from the motif, connecting the heads to the filament backbone, and shows that the backbone is built from supramolecular assemblies of myosin tails. The reconstruction provides a native structural context for understanding past biochemical and biophysical studies of this model Ca^{2+}-regulated myosin.

scallop muscle | molluscan muscle | thick-filament structure | 3D reconstruction | muscle regulation

Contractile activity in muscle is switched on and off by protein subunits on the thick (myosin-containing) and thin (actin-containing) filaments (1). Regulation via myosin is based on either Ca^{2+}-dependent phosphorylation of the myosin regulatory light chains (RLCs) (this mode of regulation occurs in vertebrate smooth muscle and some invertebrate striated muscles) or Ca^{2+} binding to the essential light chains (ELCs) (occurring in some invertebrate striated muscles) (2–6). In some muscles (vertebrate striated and some invertebrate striated), phosphorylation modulates activity but is not required for muscle activation (2, 7, 8). Electron-microscopic studies of vertebrate smooth muscle myosin molecules have revealed that, in the relaxed (dephosphorylated) state, the two myosin heads in a molecule interact with each other asymmetrically so that the actin-binding region of one (the "blocked" head) is blocked by interaction with the converter domain and ELC of the other (the "free" head). It is thought that this switches off actin-binding and ATPase activity of the blocked and free heads, respectively (9, 10), contributing to muscle relaxation. Phosphorylation of the RLC releases the two heads so that they can hydrolyze ATP and interact with actin.

In striated muscle, myosin molecules do not function as monomers, but are assembled into bipolar polymers (filaments), in which the tails form the filament backbone and the heads lie on the surface in helical arrays (11, 12). It was initially unknown whether the interacting-head conformation of isolated molecules also characterized native myosin filaments. This question was answered by cryo-electron microscopy (cryo-EM) and 3D reconstruction of filaments isolated from relaxed tarantula striated muscle, where a similar head arrangement was seen (13). This suggests that phosphorylation-regulated filaments in vivo are switched off by a similar mechanism to that proposed for isolated molecules. The filaments also showed interactions between the subfragment 2 (S2) portion of the myosin tail and the blocked head, and between heads at different axial levels of the filament (13).

The striking similarity between the head organization in isolated myosin molecules from vertebrate smooth muscle (9, 10) and in native myosin filaments from invertebrate striated muscle—two widely divergent systems—suggests that this organization is highly conserved in phosphorylation-regulated/modulated systems (13), and probably evolved before the divergence of vertebrates from invertebrates more than 600 million years ago (14). The observation of similar head–head interactions in other myosin filaments and molecules regulated or modulated by phosphorylation supports this view (15–17). Our goal here has been to answer the evolutionary question: does this interacting-head motif also characterize filaments of the other major branch of the myosin regulatory tree, in which Ca^{2+} binding to the myosin head switches on contraction (5, 6). Although support for this possibility has come from the observation of single myosin molecules (18), previous studies of filaments have suggested a very different structure, in which the heads are splayed apart from each other (19–21). Using cryo-EM and 3D reconstruction of scallop myosin filaments, we demonstrate that the interacting-head motif does indeed characterize relaxed Ca^{2+}-regulated filaments, directly demonstrating the evolutionary importance of this structure. A pseudoatomic filament model produced by atomic fitting to the reconstruction provides a 3D structural context for understanding previous biochemical and biophysical studies of Ca^{2+}-regulated myosin (reviewed in ref. 6).

Results

EM of Frozen-Hydrated Scallop Myosin Filaments. Thick filaments were purified under relaxing conditions from chemically skinned striated adductor muscle of the sea scallop *Placopecten magellanicus* (regulated by Ca^{2+} binding to the myosin heads). When observed by cryo-EM, most filaments showed relatively weak features, the most prominent being cross-striations at ~14-nm intervals (Fig. 1 *A* and *B*, and Fig. S1 *A* and *B*). An averaged power spectrum of the 16 filament halves used in the reconstruction showed layer lines extending to the 30th order (4.8 nm) of a 144-nm filament repeat (19–21) (Fig. 1*C* and Fig. S2*B*). The reflections were similar in radial and axial position to those in X-ray patterns of living scallop

Author contributions: J.L.W. and R.C. designed research; J.L.W. and F.-Q.Z. performed research; J.L.W. contributed new reagents/analytic tools; J.L.W. and R.C. analyzed data; and J.L.W. and R.C. wrote the paper.

The authors declare no conflict of interest.

This article is a PNAS Direct Submission.

[1]To whom correspondence should be addressed. E-mail: roger.craig@umassmed.edu.

This article contains supporting information online at www.pnas.org/lookup/suppl/doi:10.1073/pnas.1218462110/-/DCSupplemental.

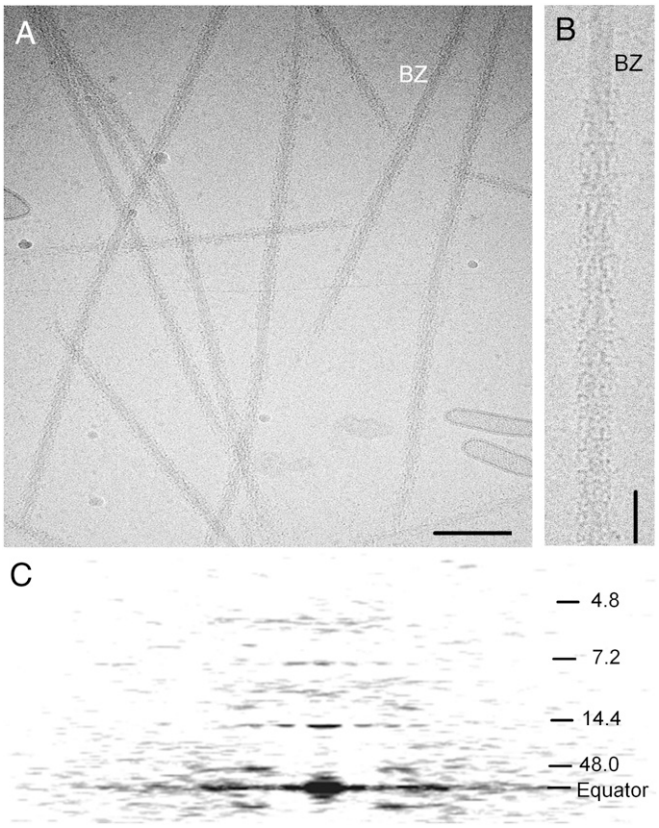

Fig. 1. Cryo-EM of scallop thick filaments. (*A*) Cryo-electron micrograph of purified filaments. BZ, bare zone. (Scale bar: 200 nm.) (*B*) Enlargement of part of one filament, bare zone at top. (Scale bar: 50 nm.) (*C*) Average power spectrum of the filaments used in the reconstruction, showing layer lines indexing on repeat of ~144 nm (19, 20). The main helical tracks give rise to a layer line at the third order of 144 nm (~48 nm) and to a meridional reflection at ~14.4 nm (10th order), corresponding to the axial spacing between crowns of myosin heads. The weak 29-nm transverse periodicity reported in negatively stained filaments (20) was only occasionally apparent in our images, in agreement with previous cryo-EM of scallop filaments (21), and with the weakness of reflections at the third and fifth orders (~5.8 and 9.6 nm) of this spacing in the power spectrum (cf. ref. 19).

muscle [Fig. S2 *A* and *B*, and Table S1 (19, 22)], suggesting that the native structure was well preserved in the cryo images. The strongest reflections were an off-meridional layer line at a spacing of 48 nm, corresponding to the axial distance between the main long-pitch myosin helices (20), and meridional reflections at 14.4 and 7.2 nm—the first and second orders of the 14.4-nm axial spacing of myosin heads (Fig. 1*C* and Fig. S2*B*).

Three-Dimensional Reconstruction of the Scallop Myosin Filament. Three-dimensional reconstruction was carried out using a single-particle approach on the 16 best filament halves (from a total of 279). Selection was based on filament straightness, appearance after helical filtration, and individual reconstruction quality. Inclusion of more filaments (of lower quality) caused the reconstruction to deteriorate, presumably due to poorer head order in the additional filaments. The resolution of the reconstruction (based on a Fourier shell correlation of 0.5) was ~5.0 nm.

The reconstruction revealed the organization of myosin heads into sevenfold symmetric "crowns" spaced 14.4 nm apart (20) (Fig. 2 and Movie S1). A clockwise 15.6° rotation between successive crowns, proceeding away from the viewer, generates seven steeply angled, coaxial, right-handed helices, creating a structure with an overall repeat of 144 nm (19–21). A density projection of the reconstruction showed features similar to those in the original micrographs (Fig. S1 *B–D*). The power spectrum of the reconstruction was also similar to that of the filaments (Fig. S2 *B* and *C*). The outside diameter of the reconstruction was ~42 nm (21), similar to the diameter directly measured in cryo-EM images (23). All of these observations support the validity of the reconstruction.

Arrangement of Myosin Heads. The most striking feature of the reconstruction was a repeating motif resembling the tilted "J" structure seen in phosphorylation-regulated filaments (Figs. 2 and 3*A*) (13, 16). In these filaments, the motif is created by the asymmetric, intramolecular interaction between the two heads of each myosin molecule. Our results suggest that a similar structure is present in Ca^{2+}-regulated filaments. However, unlike the arthropod filaments, the heads form a shell of density ~4 nm above the filament backbone, rather than closely contacting it [Fig. 4 *A* and *B* (21)], and the J-motifs are more steeply tilted and azimuthally closer together than in the arthropods (Figs. 2 and 3*A*).

Atomic Fitting. We gained insight into the molecular organization of the myosin heads by docking atomic structures of scallop myosin head and S2 tail domains into the reconstruction (Figs. 2 and 3, and Movies S1, S2, S3, and S4). The structures used were the motor domain (MD) of the prepower stroke state head [Protein Data Bank (PDB) ID code 1QVI (24)], the regulatory domain (RD) in the low-Ca^{2+} state [PDB ID code 3JTD (25)], and S2 [PDB ID code 3BAS (26)]. The fitting revealed multiple contacts between the myosin heads within a pair, between pairs within a crown, and between heads from different crowns. The head and S2 domains also came into close proximity. Although some of these contacts closely resembled those in smooth muscle, tarantula, and *Limulus*, others were different and may represent specializations of the Ca^{2+}-regulatory mechanism.

Intramolecular contacts. The regions of contact between the free and blocked scallop motor domains are essentially the same as those in the tarantula atomic model (13, 27). Thus, the actin-binding interface of the blocked head is close to the converter domain and

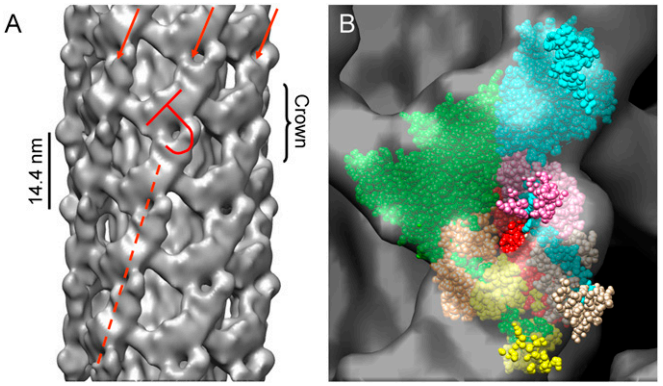

Fig. 2. Three-dimensional reconstruction and atomic fitting of scallop filament. (*A*) Longitudinal view of filament segment containing five crowns, showing paired myosin head motifs (tilted "J") in sevenfold symmetric crowns, 14.4 nm apart; three of the seven, steeply angled, right-handed helices are arrowed, and one is marked with a dashed line (Movie S1). Bare zone direction toward top; reconstruction low-pass filtered to 5-nm resolution (the calculated resolution of the reconstruction). (*B*) Fitting of space-fill atomic structures of scallop myosin head domains and S2 to one motif. The majority of the mass lies across the top of the "J" (the combined MDs) and is oriented almost along the right-handed helices (repeat ~48 nm), consistent with the prominence of the 48-nm layer line in the filament power spectrum (Fig. 1*C*) and in X-ray patterns of scallop muscle (19). The stem and curl of the J represent the two light chain domains. Green, cyan: blocked and free MDs, respectively; orange, pink: blocked and free ELCs; yellow and beige: blocked and free RLCs; red, S2. See also Movies S2, S3, and S4.

ELC of the free head (9, 13, 27) (Fig. 2*B*). In addition, as in tarantula, the N-terminal segment of S2 is close to the actin-binding cleft of the blocked MD (Fig. S3 and Movie S3), and the RLC N-lobes are also close to each other (13, 27) (Figs. 2*B* and 3*B*). A possible difference from tarantula is the close proximity of the scallop RLC C-lobes to each other and their apparent contact with S2 (Fig. 3 *B* and *C*, and Movie S3), neither of which appears to occur in tarantula. These contacts suggest possible paths for intramolecular communication that are absent in phosphorylation-regulated structures. However, the RLC domains of the tarantula model (13) were based on a skeletal model (9), and it has since been reported that a scallop model produces a better connection to S2 in this region for smooth muscle (28). Therefore, it is possible that the use of a scallop model may also introduce changes in the tarantula fit.

Intermolecular contacts. In addition to these intramolecular contacts, the head motifs also appear to make intermolecular contacts around the circumference of a crown as well as between crowns along the long-pitch helices (Fig. 3*A*). The proximity of head-pairs within a crown creates a continuous ring of contacts that appears to involve the SH3 domain of each blocked MD and the upper 50K region of the adjacent free MD. Such contacts do not occur in tarantula, where the motifs are widely separated within a crown. Along the long-pitch helices, contacts appear to occur between the actin-binding loop of the free MD and the blocked RD of the next head closer to the bare zone—specifically the Ca^{2+}-binding site in the N-lobe of the ELC and the C-lobe of the RLC, near its junction with the ELC (Fig. 3*C*). The SH3 domain of the free MD is also close to the N-lobe of the blocked RLC (Fig. 3*C*). In the tarantula structure, close contact occurred between S2 from one motif and the converter and SH3 domains of the blocked head in the next motif closer to the bare zone (13). In the scallop, the heads are above the backbone surface (Fig. 4), and these intermolecular contacts do not occur.

Filament Backbone. The reconstruction also reveals substructure in the filament backbone. In transverse view, the backbone has a polygonal appearance (Fig. 4*A*) created by an outer layer of seven repeating structures, in which the highest density (at the surface) tapers to a lower density toward the filament center. The central core of the filament shows relatively low protein density. In longitudinal view at high contour cutoff level, these structures appear to run as right-handed helices with the same pitch as the seven helices of myosin heads (Fig. 4*B*), thus pairing each with one strand of head motifs (21). When lower densities are included, the appearance becomes more complex (21) and is difficult to interpret. This appearance of "subfilaments" is consistent with previous observations (21, 29) and supports the general concept of the assembly of myosin molecules into higher order structures within thick-filament backbones. The subfilaments in the scallop are larger than the 4-nm–diameter subfilaments (containing three molecules in cross-section) seen in the arthropods (13, 30). It is possible that those in the scallop are built from such smaller (4-nm–diameter) subfilaments (Fig. 4*B*), but detailed interpretation remains speculative (29).

Discussion

Evolutionary Implications of the Reconstruction. Our 3D reconstruction shows that, in native thick filaments of the scallop, a species regulated by direct binding of Ca^{2+} to the ELC on the myosin heads, the inactive (switched-off) state is characterized by intramolecular contact between the motor domains of the two heads. It seems likely that a similar structure is also present in other species (31) regulated by Ca^{2+} binding. The contact appears to involve a similar interface to that used in switching off phosphorylation-regulated myosin filaments (13, 16) and molecules (9, 10, 17). The key conclusion from these observations, therefore, is that both major branches of the myosin regulatory tree—one regulated by RLC phosphorylation and the other by Ca^{2+} binding to the ELC—appear to depend on a similar structural mechanism for switching off myosin activity, despite their different triggers. This is supported by in vitro observations of isolated scallop myosin molecules in the off state, which show a folded-back (32), interacting-head (18) structure similar to that seen in the reconstruction, and from mutational studies suggesting an asymmetric structure for scallop myosin (33). A similar structure may also occur in unregulated (vertebrate striated) myosin filaments (15). Our findings therefore provide further critical evidence that this off-state structure is highly conserved and most likely evolved more than 600 million years ago, before vertebrates and invertebrates

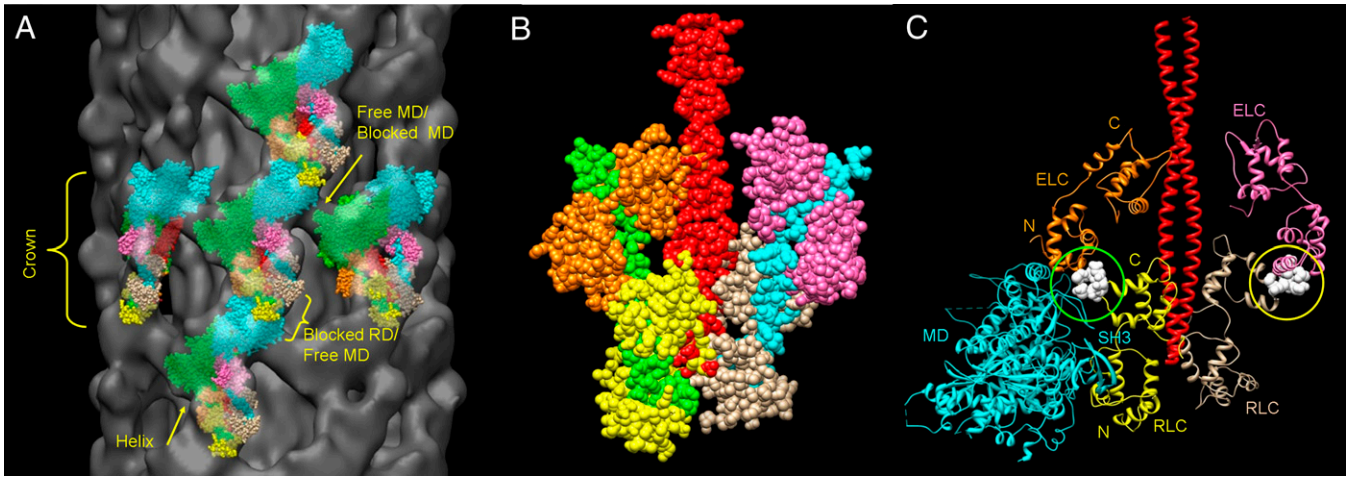

Fig. 3. Intermolecular and intramolecular contacts between myosin heads. (*A*) Fitting of scallop myosin head and S2 atomic structures to multiple motifs, showing apparent intermolecular contacts between blocked- and free-head MDs in the same crown, and between free-head MD in one crown and blocked-head RD in the next. Color scheme is as in Fig. 2. See also Movie S1. (*B*) Atomic fitting of the light chain domains suggests close proximity of the blocked- and free-head RLCs to each other (yellow, beige, respectively) at both their C and N lobes, and possible contact of the RLCs with S2 (red) in the interacting-head motif. (*C*) α-Carbon chain fit of free-head MD in one crown and RD of adjacent myosin in the same helix in next crown closer to the bare zone (HCs in regulatory domain omitted for clarity). The free-head MD in the lower crown comes close to the Ca^{2+}-binding residues of the blocked-head ELC (green-circled white spheres) in the next. The Ca^{2+}-binding site on the free head (yellow circle) is not involved in intermolecular interaction. C, N: C and N lobes of RLC and ELC.

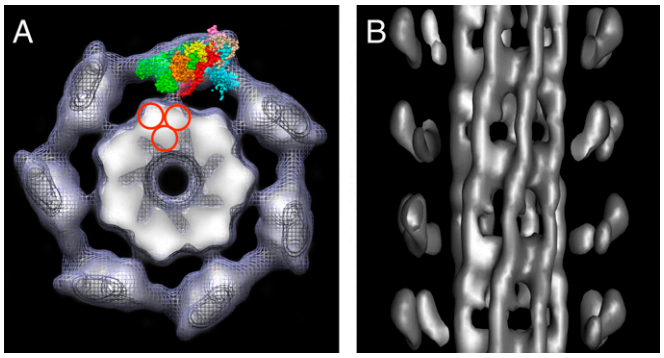

Fig. 4. Backbone structure of scallop thick filament. (*A*) Transverse combined surface mesh and density projection of one myosin head crown, viewed toward bare zone. The filament backbone consists of seven high-density (white) features (subfilaments). Density at high radius is dominated by end-on views of blocked and free motor domains of each head pair; one motif has been fitted with head and S2 atomic structures as in Fig. 2. The red circles indicate possible arrangement of 4-nm–diameter subfilaments making up the larger subfilament. (*B*) Longitudinal surface view at high contour cutoff (from subset of filaments showing backbone features especially well) reveals subfilaments running with the same right-handed twist as the myosin head helices; heads at front of filament removed to expose subfilaments. Bare zone is toward top.

diverged (13). This would suggest a common structural mechanism for switching off myosin II across most of the animal kingdom.

Relation to Previous Reconstructions. There have been three previous 3D reconstructions of scallop thick filaments. In two, based on negative stain data (20, 34), the heads were close to the filament backbone, but not individually resolved. In a preliminary cryo-EM reconstruction (21), the heads were shown to be above the backbone (as found here), suggesting that the appearance in negative stain was an artifact. It was concluded that the heads had different conformations from each other and were splayed apart axially (21), although the reconstruction did not unambiguously define the two heads. Our reconstruction resolves the heads, and atomic fitting demonstrates that they lie close together, rather than splayed apart. Fig. S4 shows how the different reconstructions can be reconciled.

Myosin Head Interactions and the Mechanism of Regulation. Because atomic structures of scallop S1 and S2 are available, we were able to build an atomic model of the scallop filament containing exclusively scallop conformations and sequences (Figs. 2*B* and 3). The hybridization and homology modeling that was required in atomic fitting of previous reconstructions was therefore avoided (13, 16, 27). In addition, the head domains were in the appropriate biochemical state [MD in ADP.Vi state (1QVI), RD in low-Ca^{2+} state (3JTD)] for the relaxed filament structure to which they were fitted. The resultant atomic model is supported by fluorescence resonance energy transfer measurements indicating that the average distance between residues 50 on the two RLCs of scallop myosin is at least 5.0 nm (35), consistent with our measured distance (also 5 nm). Cross-linking studies indicate that these RLC locations can sometimes approach as close as 0.2 nm (36), implying large excursions of the heads from their average position, consistent with the disorder seen in our cryo-images (21) and with the weakness of myosin reflections beyond 5-nm resolution in X-ray diffraction patterns of scallop muscle (19, 22).

Most of the intramolecular and intermolecular interactions involved in regulation are likely to be ionic, as regulation of scallop filaments is profoundly affected by ionic strength (37). The intramolecular interactions observed in both phosphorylation- and Ca^{2+}-regulated filaments suggest a mechanism for switching off activity in which contact between the two heads and between the blocked head and S2 contribute to myosin inhibition by physically restricting myosin head mobility (9, 13). Formation of these interactions may depend on specialized features of these myosins. Crystallographic studies show that the region of S2 near its junction with the heads is unstable in regulated myosins, consistent with the suggestion that uncoiling of approximately two heptads may be required to enable the heads to adopt their asymmetric, interacting positions in the off state (26, 38–40). X-ray studies of the scallop RD suggest that formation of these interactions may also depend on increased flexibility of the regulatory domain heavy chain (HC) that results from reduction in the interaction of the ELC with the RLC upon loss of Ca^{2+} (25). Our fitting suggests close contact between the two RLCs and between the RLCs and S2 (Fig. 3*C*), which may stabilize these flexible regions of S2 and the RD in the relaxed filament (Fig. 3*C*), forming a possible off-state "regulatory complex." Interaction of the N lobes of the two RLCs could modulate the mechanical characteristics of the head/rod junctional region and provide a structural pathway for communicating activation/relaxation signals between heads (6). Stiffening of the RD upon Ca^{2+} binding (25) may disrupt RLC–RLC and RLC–S2 interactions, in turn reducing the stabilization of the unwound N-terminal region of S2 (26) and leading to the increased freedom of movement of the heads that occurs when scallop myosin is activated (32). Thus, activation may result not from transmission of a directed conformational change along the myosin heads from the RLC region to the head–head interface, but from increased thermal motion of the heads made possible by an increase in flexibility of the head/rod junction.

Although the intramolecular interactions between heads appear similar in Ca^{2+}- and phosphorylation-regulated filaments, intermolecular contacts, within crowns and along helical tracks (Fig. 3*A*), are different and may represent specializations of the Ca^{2+}-regulatory system. These contacts—not present in single molecules (18)—may further shut down myosin activity and could contribute to the structural mechanism underlying the "super-relaxed" state thought to be present in scallop and other species, in which ATP turnover by myosin filaments is highly inhibited (41). Proximity of the free head MD in one crown to the ELC Ca^{2+}-binding residues of the blocked head in the next crown (Fig. 3*C*) may impede Ca^{2+} binding to the blocked head. Upon activation, Ca^{2+} may bind initially to the free heads, where access is unimpaired. If this weakens their various interactions, these heads may become more mobile, allowing Ca^{2+} to bind more readily to the blocked heads, thus leading to cooperative activation of the filament as a whole (6, 42). A similar sequence of free and blocked head activation has been proposed for tarantula filaments based on the differential accessibility of myosin light chain kinase to phosphorylation sites on the free- and blocked-head RLCs (43).

The significant degree of head disorder seen in individual scallop filament images and implied by the low resolution of scallop muscle X-ray diffraction patterns suggests that the relaxed interactions between heads are relatively weak. The additive effect of multiple, weak interactions appears to keep the filament switched off (13), and may also be a requirement for the rapid activation that occurs when Ca^{2+} levels rise (44). When scallop filaments are activated by Ca^{2+}, the myosin heads become disordered on the millisecond timescale (23), consistent with breaking of the head–head and other interactions, allowing free head movement and interaction with actin. The rapid reordering of heads that occurs upon relaxation (45) suggests that the structure and interactions that we have described are essential features of the relaxed state.

Relation to Vertebrate Smooth Muscle Thick Filaments. The thick filaments of vertebrate smooth muscle have a nonhelical, "side-polar" structure in which heads on opposite sides have opposite polarity (46, 47). Although the heads in relaxed filaments

presumably have similar intramolecular interactions to those in molecules (9), this has not yet been demonstrated, owing to the lability of these filaments, and potential intermolecular interactions remain unknown. The close relationship between vertebrate smooth and scallop striated muscle myosin (6, 18, 25, 28, 48), together with certain structural similarities between scallop and smooth muscle filaments, suggests that the scallop reconstruction may hold clues to molecular organization in the side-polar structure. The packing of myosin heads within a crown in the scallop is much tighter than in other striated muscle filaments (13, 15, 16), leading to azimuthal contacts between neighboring blocked and free motor domains that are absent from these other systems (Fig. 3*A*). Geometric considerations (47, 49, 50) suggest similarly tight packing in side-polar filaments, which might thus involve similar azimuthal interactions to those in scallop. Tomographic reconstruction of smooth muscle filaments will be required to test this prediction.

Conclusions

The results of this study fill a crucial gap in our understanding of the evolution of muscle regulation. Our reconstruction suggests that the shutting down of myosin filament activity that leads to relaxation is accomplished through a similar structural mechanism in both major branches of the myosin regulatory tree (phosphorylation and Ca^{2+} binding). Not only is the interacting head motif similar in both systems at the filament (13, 16) and single-molecule (18) level, but crystallographic studies of the RD suggest that the mechanism of activation may also be similar, although with different triggers (25). Recent genome-mining studies suggest that phosphorylation of the RLC by myosin light chain kinase is the most ancient mechanism for regulating actomyosin interaction (51). This mechanism must have sufficed for early, slowly contracting muscles, and persists today in nonmuscle, smooth muscle, and primitive striated muscle contractile systems (51). However, the slow speed of such an enzymatic reaction would not be adequate for striated muscles dependent on a rapid twitch response. It thus appears likely that the relaxed head–head interaction may have evolved in molluscs [and other species regulated by Ca^{2+} binding to myosin (31)] as a rapidly activatable adaptation of the early, phosphorylation-dependent structure. Other species have solved the rapid response problem by switching regulation to the thin filaments, where troponin rapidly binds and releases Ca^{2+} (1). In these systems, the relatively slow response brought about by enzymatically induced RLC phosphorylation has been retained but is used here to modulate contractility on a longer timescale (2).

Materials and Methods

EM. Scallops (*Placopecten magellanicus*) were obtained from the Marine Biological Laboratory and stored in a marine aquarium at 12 °C. Myosin filaments were purified from the striated portion of the adductor muscle by detergent skinning of small fiber bundles in relaxing medium [100 mM NaCl, 3 mM $MgCl_2$, 5 mM MgATP, 1 mM EGTA, 5 mM Pipes, 5 mM NaH_2PO_4, 1 mM NaN_3 (pH 7.0)], followed by brief homogenization, centrifugation, and resuspension (23). Specimens were prepared for cryo-EM by applying 6 μL of filament suspension to a holey carbon grid, blotting to a thin film, and then plunging into liquid ethane (23). Grids were examined at 120 kV under low-dose conditions in a Philips CM120 cryo-electron microscope (FEI) using a Gatan 626 DH cryoholder at approximately −184 °C. Images of filaments suspended in vitreous ice over holes in the carbon film were recorded under low-dose conditions on Kodak S0163 film at a magnification of 35,000× and defocus of ∼1.5 μm. A second image, used to determine filament quality, was then obtained at 4.6-μm defocus.

Image Processing. EM negatives were scanned on an Imacon FlexTight Precision scanner (Hasselblad) to give a pixel size of 0.51 nm in the original image. Each half-filament was oriented with the bare zone at the top to ensure correct relative polarity. Fast Fourier transforms and their averages were computed with ImageJ (W. S. Rasband, ImageJ, National Institutes of Health, Bethesda, MD; http://imagej.nih.gov/ij/; 1997–2011). Three-dimensional reconstruction was carried out on individual filament halves by single-particle methods using the SPIDER software package (52), assuming myosin head crowns with a rotational symmetry of 7, an axial rise of 14.4 nm between crowns, and a repeat of 48.0 nm (19–21) (*SI Materials and Methods*). Owing to possible perturbations in the myosin helix (20), only regions at least 150 nm from the bare zone and the filament tip were used. Individual reconstructions were aligned using University of California, San Francisco (UCSF) Chimera (53), and then averaged in SPIDER. The final average was based on images from 16 filament halves, selected from an original 279 on the basis of straightness, appearance after helical filtration (clear 14.4-nm myosin head cross-striation and 48-nm-spaced oblique lines, indicating helical preservation), and individual reconstruction quality. The reconstruction contained information from 402 filament segments, each 72.5 nm long, with a stagger of 14.4 nm between segments from the same filament. The total number of unique pairs of myosin heads that went into the reconstruction was 3,260. Reconstructions were rendered using Chimera (53).

Computational Fitting. Docking of atomic models into the reconstruction was carried out manually within Chimera (53). The limited (∼5.0-nm) resolution of the reconstruction precluded unambiguous fitting of individual motor and regulatory domains in a single step [which had been possible when fitting the higher-resolution tarantula and *Limulus* reconstructions (13, 16)]. A two-step procedure was therefore used. Preliminary fitting was carried out using hybrid atomic models for the complete interacting-head motif derived from smooth muscle heavy meromyosin (PDB ID code 1I84) (9) or tarantula myosin filaments (PDB ID code 3DTP) (27). The best fit of the interacting motor domains (obtained with 3DTP) was then used as a template for fitting the MDs of the prepower stroke scallop head [1QVI (24)]. The Ca^{2+}-free scallop RD [3JTD (25)] was then fitted into the reconstruction density of each head while ensuring that its N-terminal HC correctly matched up to the HC of each MD, and that its C-terminal HC correctly joined the α helices at the N terminal of the scallop S2 tail structure [3BAS (26)]. Minor adjustments were then made to optimize the fit, resulting in a final homogeneous atomic model containing only scallop structures (*SI Materials and Methods*).

ACKNOWLEDGMENTS. This work was supported by National Institutes of Health (NIH) Grants R01 AR034711 (to R.C.) and P01 HL059408 (to D. Warshaw). EM was carried out in the Core Electron Microscopy Facility of the University of Massachusetts Medical School. Molecular graphics images were produced using the UCSF Chimera package from the Resource for Biocomputing, Visualization, and Informatics at UCSF (supported by NIH Grant P41 RR-01081).

1. Gordon AM, Homsher E, Regnier M (2000) Regulation of contraction in striated muscle. *Physiol Rev* 80(2):853–924.
2. Sweeney HL, Bowman BF, Stull JT (1993) Myosin light chain phosphorylation in vertebrate striated muscle: Regulation and function. *Am J Physiol* 264(5 Pt 1):C1085–C1095.
3. Trybus KM (1994) Role of myosin light chains. *J Muscle Res Cell Motil* 15(6):587–594.
4. Sellers JR (1981) Phosphorylation-dependent regulation of Limulus myosin. *J Biol Chem* 256(17):9274–9278.
5. Szent-Györgyi AG (1975) Calcium regulation of muscle contraction. *Biophys J* 15(7): 707–723.
6. Chantler PD (2006) *Scallops: Biology, Ecology and Aquaculture*, eds Shumway SE, Parsons GJ (Elsevier, Amsterdam), pp 231–320.
7. Craig R, Padrón R, Kendrick-Jones J (1987) Structural changes accompanying phosphorylation of tarantula muscle myosin filaments. *J Cell Biol* 105(3):1319–1327.
8. Stull JT, Kamm KE, Vandenboom R (2011) Myosin light chain kinase and the role of myosin light chain phosphorylation in skeletal muscle. *Arch Biochem Biophys* 510(2): 120–128.
9. Wendt T, Taylor D, Trybus KM, Taylor K (2001) Three-dimensional image reconstruction of dephosphorylated smooth muscle heavy meromyosin reveals asymmetry in the interaction between myosin heads and placement of subfragment 2. *Proc Natl Acad Sci USA* 98(8):4361–4366.
10. Burgess SA, et al. (2007) Structures of smooth muscle myosin and heavy meromyosin in the folded, shutdown state. *J Mol Biol* 372(5):1165–1178.
11. Huxley HE (1963) Electron microscope studies on the structure of natural and synthetic protein filaments from striated muscle. *J Mol Biol* 7(3):281–308.
12. Craig R, Woodhead JL (2006) Structure and function of myosin filaments. *Curr Opin Struct Biol* 16(2):204–212.
13. Woodhead JL, et al. (2005) Atomic model of a myosin filament in the relaxed state. *Nature* 436(7054):1195–1199.
14. Peterson KJ, et al. (2004) Estimating metazoan divergence times with a molecular clock. *Proc Natl Acad Sci USA* 101(17):6536–6541.
15. Zoghbi ME, Woodhead JL, Moss RL, Craig R (2008) Three-dimensional structure of vertebrate cardiac muscle myosin filaments. *Proc Natl Acad Sci USA* 105(7):2386–2390.

16. Zhao FQ, Craig R, Woodhead JL (2009) Head-head interaction characterizes the relaxed state of Limulus muscle myosin filaments. *J Mol Biol* 385(2):423–431.
17. Jung HS, Komatsu S, Ikebe M, Craig R (2008) Head-head and head-tail interaction: A general mechanism for switching off myosin II activity in cells. *Mol Biol Cell* 19(8): 3234–3242.
18. Jung HS, et al. (2008) Conservation of the regulated structure of folded myosin 2 in species separated by at least 600 million years of independent evolution. *Proc Natl Acad Sci USA* 105(16):6022–6026.
19. Wray JS, Vibert PJ, Cohen C (1975) Diversity of cross-bridge configurations in invertebrate muscles. *Nature* 257(5527):561–564.
20. Vibert P, Craig R (1983) Electron microscopy and image analysis of myosin filaments from scallop striated muscle. *J Mol Biol* 165(2):303–320.
21. Vibert P (1992) Helical reconstruction of frozen-hydrated scallop myosin filaments. *J Mol Biol* 223(3):661–671.
22. Millman BM, Bennett PM (1976) Structure of the cross-striated adductor muscle of the scallop. *J Mol Biol* 103(3):439–467.
23. Zhao FQ, Craig R (2003) Ca^{2+} causes release of myosin heads from the thick filament surface on the milliseconds time scale. *J Mol Biol* 327(1):145–158.
24. Gourinath S, et al. (2003) Crystal structure of scallop myosin S1 in the pre-power stroke state to 2.6 Å resolution: Flexibility and function in the head. *Structure* 11(12): 1621–1627.
25. Himmel DM, Mui S, O'Neall-Hennessey E, Szent-Györgyi AG, Cohen C (2009) The on-off switch in regulated myosins: Different triggers but related mechanisms. *J Mol Biol* 394(3):496–505.
26. Brown JH, et al. (2008) An unstable head-rod junction may promote folding into the compact off-state conformation of regulated myosins. *J Mol Biol* 375(5):1434–1443.
27. Alamo L, et al. (2008) Three-dimensional reconstruction of tarantula myosin filaments suggests how phosphorylation may regulate myosin activity. *J Mol Biol* 384(4): 780–797.
28. Baumann BA, et al. (2012) Phosphorylated smooth muscle heavy meromyosin shows an open conformation linked to activation. *J Mol Biol* 415(2):274–287.
29. Castellani L, Vibert P (1992) Location of paramyosin in relation to the subfilaments within the thick filaments of scallop striated muscle. *J Muscle Res Cell Motil* 13(2): 174–182.
30. Wray JS (1979) Structure of the backbone in myosin filaments of muscle. *Nature* 277(5691):37–40.
31. Lehman W, Szent-Györgyi AG (1975) Regulation of muscular contraction. Distribution of actin control and myosin control in the animal kingdom. *J Gen Physiol* 66(1):1–30.
32. Stafford WF, et al. (2001) Calcium-dependent structural changes in scallop heavy meromyosin. *J Mol Biol* 307(1):137–147.
33. Colegrave M, Patel H, Offer G, Chantler PD (2003) Evaluation of the symmetric model for myosin-linked regulation: Effect of site-directed mutations in the regulatory light chain on scallop myosin. *Biochem J* 374(Pt 1):89–96.
34. AL-Khayat HA, Morris EP, Squire JM (2009) The 7-stranded structure of relaxed scallop muscle myosin filaments: Support for a common head configuration in myosin-regulated muscles. *J Struct Biol* 166(2):183–194.
35. Chantler PD, Tao T, Stafford WF, 3rd (1991) On the relationship between distance information derived from cross-linking and from resonance energy transfer, with specific reference to sites located on myosin heads. *Biophys J* 59(6):1242–1250.
36. Bower SM, Wang Y, Chantler PD (1992) Regulatory light-chain Cys-55 sites on the two heads of myosin can come within 2Å of each other. *FEBS Lett* 310(2):132–134.
37. Nyitrai M, Stafford WF, Szent-Györgyi AG, Geeves MA (2003) Ionic interactions play a role in the regulatory mechanism of scallop heavy meromyosin. *Biophys J* 85(2): 1053–1062.
38. Li Y, et al. (2003) Visualization of an unstable coiled coil from the scallop myosin rod. *Nature* 424(6946):341–345.
39. Tama F, Feig M, Liu J, Brooks CL, 3rd, Taylor KA (2005) The requirement for mechanical coupling between head and S2 domains in smooth muscle myosin ATPase regulation and its implications for dimeric motor function. *J Mol Biol* 345(4):837–854.
40. Blankenfeldt W, Thomä NH, Wray JS, Gautel M, Schlichting I (2006) Crystal structures of human cardiac beta-myosin II S2-Delta provide insight into the functional role of the S2 subfragment. *Proc Natl Acad Sci USA* 103(47):17713–17717.
41. Stewart MA, Franks-Skiba K, Chen S, Cooke R (2010) Myosin ATP turnover rate is a mechanism involved in thermogenesis in resting skeletal muscle fibers. *Proc Natl Acad Sci USA* 107(1):430–435.
42. Chantler PD, Sellers JR, Szent-Györgyi AG (1981) Cooperativity in scallop myosin. *Biochemistry* 20(1):210–216.
43. Brito R, et al. (2011) A molecular model of phosphorylation-based activation and potentiation of tarantula muscle thick filaments. *J Mol Biol* 414(1):44–61.
44. Rall JA (1981) Mechanics and energetics of contraction in striated muscle of the sea scallop, *Placopecten magellanicus*. *J Physiol* 321:287–295.
45. Zhao FQ, Craig R (2008) Millisecond time-resolved changes occurring in Ca^{2+}-regulated myosin filaments upon relaxation. *J Mol Biol* 381(2):256–260.
46. Craig R, Megerman J (1977) Assembly of smooth muscle myosin into side-polar filaments. *J Cell Biol* 75(3):990–996.
47. Xu JQ, Harder BA, Uman P, Craig R (1996) Myosin filament structure in vertebrate smooth muscle. *J Cell Biol* 134(1):53–66.
48. Sellers JR, Chantler PD, Szent-Györgyi AG (1980) Hybrid formation between scallop myofibrils and foreign regulatory light-chains. *J Mol Biol* 144(3):223–245.
49. Squire JM (1973) General model of myosin filament structure. 3. Molecular packing arrangements in myosin filaments. *J Mol Biol* 77(2):291–323.
50. Tonino P, Simon M, Craig R (2002) Mass determination of native smooth muscle myosin filaments by scanning transmission electron microscopy. *J Mol Biol* 318(4): 999–1007.
51. Steinmetz PR, et al. (2012) Independent evolution of striated muscles in cnidarians and bilaterians. *Nature* 487(7406):231–234.
52. Frank J, et al. (1996) SPIDER and WEB: Processing and visualization of images in 3D electron microscopy and related fields. *J Struct Biol* 116(1):190–199.
53. Pettersen EF, et al. (2004) UCSF Chimera—a visualization system for exploratory research and analysis. *J Comput Chem* 25(13):1605–1612.

Supporting Information

Woodhead et al. 10.1073/pnas.1218462110

SI Materials and Methods

Three-Dimensional Reconstruction Procedure. Three-dimensional reconstruction of scallop filaments was carried out using a modified single-particle approach. Initially, we used the iterative helical real space reconstruction (IHRSR) technique (1), in which filament images are computationally cut into short segments, which are matched against projections of a model with the correct symmetry, rotated about the filament axis at 4° intervals. The angle of best match determined by correlation methods is used in computing backprojections of the images to provide a 3D reconstruction, which is then helically averaged. This reconstruction is used as a new model, and the process is iterated until there is no further change in the reconstruction. This approach was straightforward for negatively stained scallop filaments and gave a 3D reconstruction with ~6-nm resolution, similar in appearance to published reconstructions based on negative staining (2, 3) (Fig. S4*A*).

However, the same procedure failed with unstained, frozen-hydrated filaments. The high level of symmetry (sevenfold rotational symmetry), together with the high intrinsic noise and low contrast of the images, caused the projection matching to fail, as many of the different views of the segments looked very similar to each other. In addition, the subfilament structure of the backbone tended to dominate the projections so that head alignment was compromised. We therefore used a different approach. Using knowledge of their symmetry (2, 4, 5), it is possible to compute reconstructions of individual filaments by a modified IHRSR procedure. Backprojection angles are assigned to each segment based on this known symmetry rather than on projection matching to a model. Reconstructions of individual half-filaments were computed in this way and helically averaged. The resulting reconstructions were aligned in Chimera, and then averaged in SPIDER (using the Chimera alignment parameters) to generate a final reconstruction.

Reconstruction Statistics and Resolution. The reconstruction was based on the 16 best filament halves (chosen from a total of 279), each containing an average of 25 segments, 72-nm (i.e., five crowns) long. Individual segments used in the reconstruction were staggered by 14.4 nm (one crown); thus, ~25 + 5 = 30 unique crowns (=210 unique motifs due to sevenfold symmetry) were averaged per half-filament. The total number of unique motifs used in the reconstruction was therefore ~3,360. The reconstruction had a resolution of ~5 nm according to the Fourier shell correlation using a 0.5 threshold. This is comparable to the resolution obtained in a previous scallop filament cryo-reconstruction (5) and similar to the highest resolution myosin reflections reported in X-ray diffraction patterns of living scallop muscle (4, 6), suggesting substantial mobility of the myosin heads in this muscle in vivo (5). Thus, the limited resolution of the reconstruction appears to reflect intrinsic motions of the heads rather than problems of specimen preparation, imaging, or reconstruction (5). The power spectrum of the reconstruction filtered to this resolution is similar to the averaged power spectrum of the filament images used in the reconstruction and to the myosin component of the X-ray patterns (Fig. S2), supporting the validity of the reconstruction.

Atomic Fitting. Although the resolution of the reconstruction was relatively limited, atomic fitting was substantially constrained by the requirement of fitting multiple asymmetric motifs within the helical tracks. Fitting was carried out in two stages. The volume and shape of the head-pair motif in the reconstruction was broadly similar to those of the interacting-head structure in the smooth muscle heavy meromyosin and tarantula filament models [Protein Data Bank (PDB) ID codes 1I84 and 3DTP, respectively]; the main density was along the top of the motif and must therefore represent the MDs of the two heads. A good fit to this region of the motif was obtained for the two motor domains linked as a single rigid body, using both the smooth muscle and tarantula models, with tarantula giving the better fit of the two. Tarantula also gave the better fit when the two regulatory domains were fitted to the motif as a single rigid body, separate from the motor domains. However, the best fit for the combined motor domains was not compatible with the best fit for the combined regulatory domains without significant modification. This precluded a good global fit into the motif for either of the complete atomic models (i.e., including all four domains as a single rigid body). We therefore first fitted the two tarantula motor domains as a single rigid body, and then each of the regulatory domains as individual rigid bodies, to obtain an overall initial best fit. In addition to the boundaries imposed by the density envelope of the reconstruction, each regulatory domain was constrained so that the N terminal of the heavy chain remained adjacent to the C terminal of its corresponding motor domain heavy chain. The approximate fit obtained in this way with the tarantula structure was used as a template for initial alignment of the relaxed state (prepower stroke) scallop atomic model for the motor domains derived from scallop S1.ADP.Vi (PDB ID code 1QVI) (7) truncated at heavy chain residue Met-773 [within the pliant point region, where significant flexibility has been reported (8)]. The regulatory domain of this structure was not used because the S1 had been crystallized in the presence of Ca^{2+} and the regulatory domain may therefore have had a different conformation from that in the relaxed state. Instead, an atomic model of the Ca^{2+}-free scallop regulatory domain (PDB ID code 3JTD) (9) was used to replace the regulatory domains in the fitted tarantula model. [Indeed, when the ELC region of 1QVI (containing Ca^{2+} bound to the ELC) was superimposed on the tarantula template, the N-terminal domain of the RLC projected out of the density envelope. When the Ca^{2+}-free (off-state) RD (3JTD) ELC region was superimposed over the Ca^{2+}-bound RD, the RLC was then found to stay within the density envelope, consistent with the expectation that an ADP.Vi MD/Ca^{2+}-free RD model should give the best fit to the relaxed filament.] Both the motor and regulatory domain models were then readjusted within the density envelope to achieve the best final fit while retaining correct heavy chain continuity between regulatory and motor domains within each head. Finally, the remaining density joining the two S1 regions to the filament backbone was fitted with an atomic model of the N-terminal region of scallop myosin S2 (PDB ID code 3BAS) (10) while ensuring that the C-terminal heavy chain truncation points were in close proximity at the head–rod junction.

1. Egelman EH (2000) A robust algorithm for the reconstruction of helical filaments using single-particle methods. *Ultramicroscopy* 85(4):225–234.

2. Vibert P, Craig R (1983) Electron microscopy and image analysis of myosin filaments from scallop striated muscle. *J Mol Biol* 165(2):303–320.

3. AL-Khayat HA, Morris EP, Squire JM (2009) The 7-stranded structure of relaxed scallop muscle myosin filaments: Support for a common head configuration in myosin-regulated muscles. *J Struct Biol* 166(2):183–194.
4. Wray JS, Vibert PJ, Cohen C (1975) Diversity of cross-bridge configurations in invertebrate muscles. *Nature* 257(5527):561–564.
5. Vibert P (1992) Helical reconstruction of frozen-hydrated scallop myosin filaments. *J Mol Biol* 223(3):661–671.
6. Millman BM, Bennett PM (1976) Structure of the cross-striated adductor muscle of the scallop. *J Mol Biol* 103(3):439–467.
7. Gourinath S, et al. (2003) Crystal structure of scallop myosin S1 in the pre-power stroke state to 2.6 Å resolution: Flexibility and function in the head. *Structure* 11(12):1621–1627.
8. Houdusse A, Szent-Györgyi AG, Cohen C (2000) Three conformational states of scallop myosin S1. *Proc Natl Acad Sci USA* 97(21):11238–11243.
9. Himmel DM, Mui S, O'Neall-Hennessey E, Szent-Györgyi AG, Cohen C (2009) The on-off switch in regulated myosins: Different triggers but related mechanisms. *J Mol Biol* 394(3):496–505.
10. Brown JH, et al. (2008) An unstable head-rod junction may promote folding into the compact off-state conformation of regulated myosins. *J Mol Biol* 375(5):1434–1443.

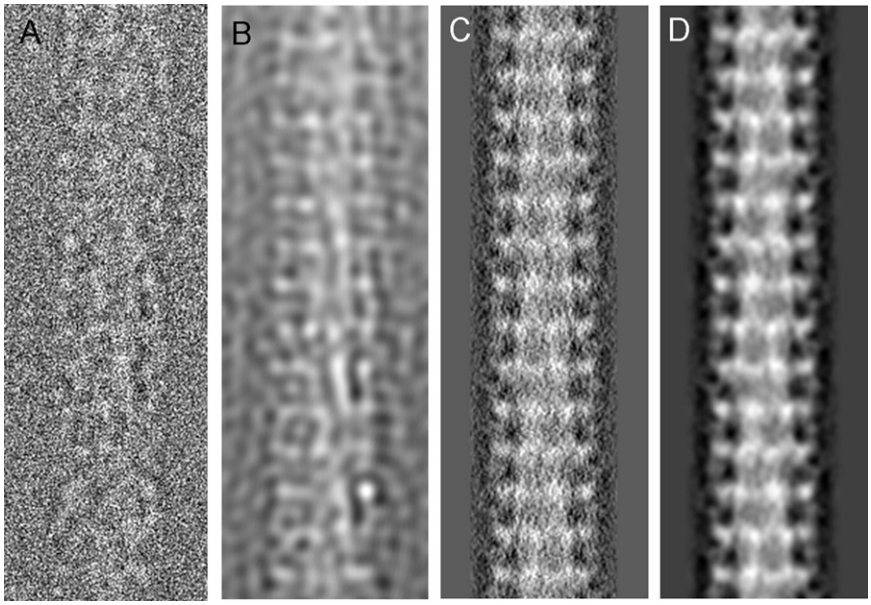

Fig. S1. Comparison of reconstruction with filament images. (*A*) Raw image at 4.6-μm defocus; (*B*) same as *A* but with high-frequency noise removed by Fourier filtration; (*C*) projection of reconstruction; (*D*) same as *C* but Fourier filtered to ∼5-nm resolution. The features in the final reconstruction are consistent with the original images (cf. also Fig. S2). *A* and *B* are in reverse contrast (protein white) for consistency with *C* and *D*.

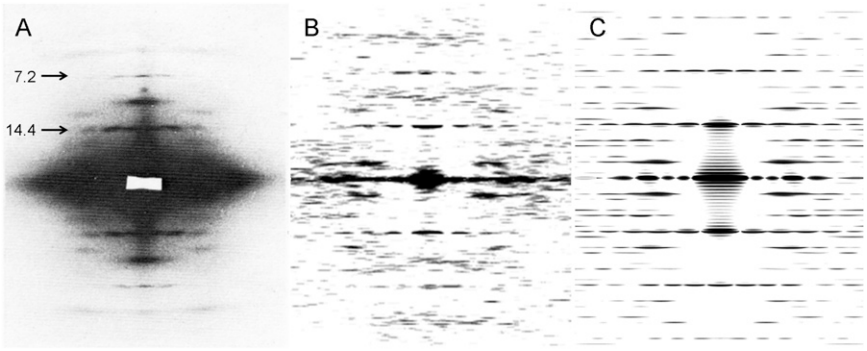

Fig. S2. Comparison of X-ray diffraction pattern of live scallop muscle (*A*) (1) with power spectra of the filaments used in reconstruction (*B*) and of the reconstruction itself (*C*). The computed intensities from the filaments agree well in axial and radial position with those from the X-ray pattern (Table S1), implying good preservation of native structure in the cryo-EM images. The good correspondence between the patterns in *B* and *C* supports the validity of the reconstruction. The arrows indicate 14.4- and 7.2-nm reflections. *A* was originally published in *Nature*. Reprinted by permission from Macmillan Publishers Ltd: *Nature* (1), Copyright (1975).

1. Wray JS, Vibert PJ, Cohen C (1975) Diversity of cross-bridge configurations in invertebrate muscles. *Nature* 257(5527):561–564, http://www.nature.com/nature/index.html.

Fig. S3. Position of S2 in the reconstruction, showing relationship to actin-binding cleft on blocked MD (colors as in Fig. 2*B*).

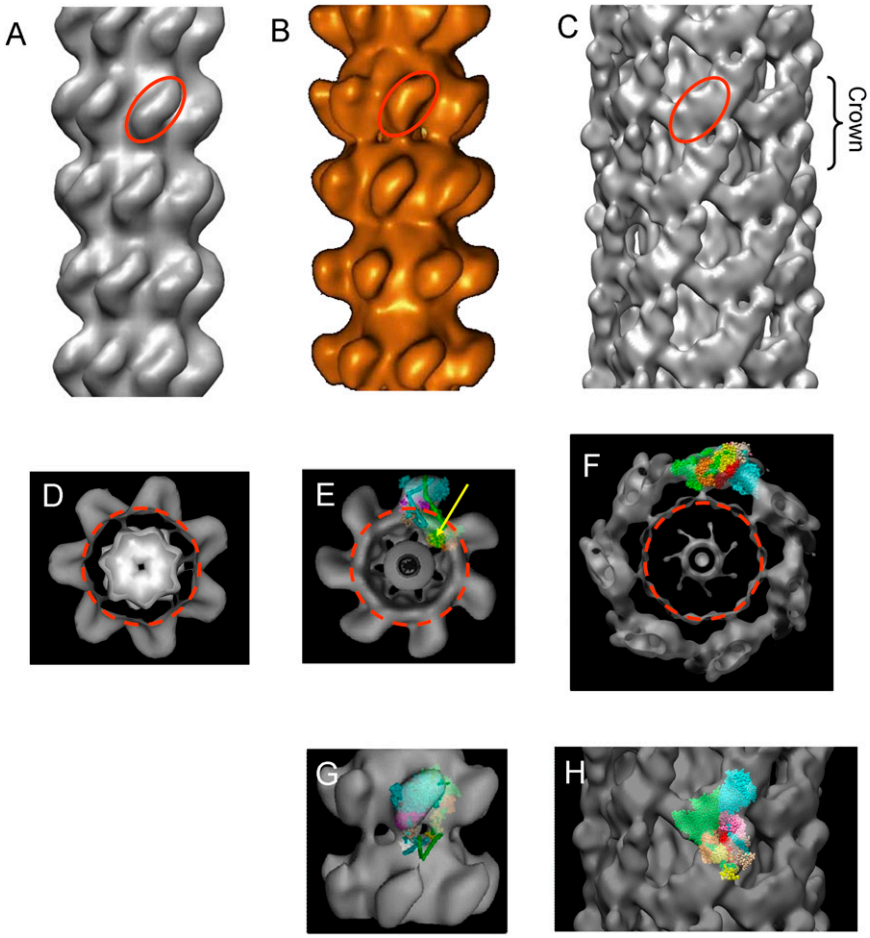

Fig. S4. Reconciling the reconstruction with previous scallop thick-filament reconstructions. Longitudinal (*A*–*C*, *G*, and *H*) and transverse (*D*–*F*) views of negative stain (*A*, *B*, *D*, *E*, and *G*) and cryo (*C*, *F*, and *H*) reconstructions, all on same scale. Bare zone up in *A*–*C*, *G*, and *H*; looking toward bare zone in *D*–*F*. The first reconstruction of scallop thick filaments (using negative staining combined with helical reconstruction methods) revealed a right-handed, helical organization of elongated motifs with sevenfold rotational symmetry (1). We (*A*) and AL-Khayat et al. [*B* (2)] obtained similar negative stain reconstructions to (1) using single-particle techniques. Comparison with the cryo-reconstruction (*C* and *H*) suggests that the repeating motif in the negative stain structures (red oval) corresponds only to the combined motor domains of the two heads (the strongest feature of the cryo-reconstruction) and that the weaker regulatory domains are not visualized. In the negative stain reconstructions, the heads appear to fuse with the backbone [*A*, *B*, *D*, and *E* (1, 2)], whereas in the cryo-reconstruction, they lie in a shell above it [*F* (3)]. This suggests that the heads collapse on to the backbone during the staining procedure, although there appears to be little shrinkage of the backbone itself (red circle in *D*–*F*). This collapse is reflected in a smaller filament diameter in the negative stain compared with the cryo-reconstructions (compare *A*, *B*, *D*, and *E*, with *C* and *F*), and in the original images [37-nm diameter in negative stain compared with 42-nm by cryo (4)]. In the negative stain reconstructions, detail is insufficient to resolve individual myosin heads [*A*, *B*, *D*, and *E* (1)], making interpretation of their organization highly speculative [resolution in ref. 1 is 7 nm and in ref. 2 is 6.5 nm (according to Fourier shell correlation 0.5 criterion)]. In ref. 1, it was suggested that the heads lay parallel to each other pointing away from the bare zone. In ref. 2, the structure was interpreted in terms of the interacting-head atomic model (5), but one of the heads (the blocked head) was placed at very low radius, where it would be inside the filament backbone (yellow arrow in *E*); in addition, there are no apparent intermolecular contacts along the long-pitch helices. We find that both heads are positioned above the backbone, oriented very differently from those in ref. 2 (compare *G* with *H*) and make multiple contacts along the helices. In the previous cryo-EM study of scallop filaments (3), it was concluded that the heads had different conformations from each other and were splayed apart axially. However, the reconstruction did not unambiguously define the two heads and was carried out before myosin head atomic structures were available, precluding definitive interpretation. Analysis of our reconstruction shows that the apparent splayed structure, with one head (further from the bare zone) "less massive" than the other (3), is a misinterpretation of what is actually the interacting head motif seen in side view. The less dense "head" (further from the bare zone) is a projection of the RDs and the denser "head" is a projection of the (larger) MDs in a single motif. The images in *B*, *E*, and *G* were originally published in the *Journal of Structural Biology*. Reprinted from the *Journal of Structural Biology*, 166/2, AL-Khayat, HA, Morris, EP, Squire, JM, The 7-stranded structure of relaxed scallop muscle myosin filaments: Support for a common head configuration in myosin-regulated muscles, 183–194, Copyright (2009), with permission from Elsevier.

1. Vibert P, Craig R (1983) Electron microscopy and image analysis of myosin filaments from scallop striated muscle. *J Mol Biol* 165(2):303–320.
2. AL-Khayat HA, Morris EP, Squire JM (2009) The 7-stranded structure of relaxed scallop muscle myosin filaments: Support for a common head configuration in myosin-regulated muscles. *J Struct Biol* 166(2):183–194, http://www.sciencedirect.com/science/journal/10478477.
3. Vibert P (1992) Helical reconstruction of frozen-hydrated scallop myosin filaments. *J Mol Biol* 223(3):661–671.
4. Zhao FQ, Craig R (2003) Ca^{2+} causes release of myosin heads from the thick filament surface on the milliseconds time scale. *J Mol Biol* 327(1):145–158.
5. Wendt T, Taylor D, Trybus KM, Taylor K (2001) Three-dimensional image reconstruction of dephosphorylated smooth muscle heavy meromyosin reveals asymmetry in the interaction between myosin heads and placement of subfragment 2. *Proc Natl Acad Sci USA* 98(8):4361–4366.

Table S1. Comparison of X-ray patterns of live scallop muscle with averaged Fourier transform of frozen-hydrated scallop thick filaments

Layer line spacing, nm (order)*	Axial spacing, nm (Wray/Millman)†	Axial spacing, nm (this work)	Radial spacings of off-meridional reflections, nm‡ (Wray/Millman)	Radial spacings,‡ nm (this work)
48.0 (3)	48.7/46.4	48.5	NM§/14.3	12.3
20.6 (7)	20.8/20.0	20.5	NM/14.0	10.2
14.4 (10)	14.6/14.5	14.4¶	27.0, 14.5/27.8, 14.3	23.9, 13.1
11.2 (13)	11.2/11.2	11.0	13.0/13.5	12.9
7.25 (20)	7.3/7.26	7.16	36.5, 16.5/35.9, NR‖	31.9, 15.3

This table compares the axial and radial positions of reflections in X-ray diffraction patterns of live scallop muscle with those in the averaged Fourier transform of the frozen hydrated scallop filaments used in this study. Note the excellent agreement between the axial spacings. It is possible that the imperfect correspondence between spacings in the radial direction is due in part to lattice sampling effects in the X-ray pattern that are absent in single filaments (1).

*Nominal layer line spacing in nanometers and order of 144-nm repeat.

†Spacing of reflection measured in X-ray diffraction patterns of live scallop muscle: Wray et al. (2) and Millman et al. (1).

‡Some layer lines have multiple reflections at different radial positions.

§Not measurable in pattern.

¶Assumed. Other spacings are based on this as an internal calibration.

‖Not reported.

1. Millman BM, Bennett PM (1976) Structure of the cross-striated adductor muscle of the scallop. *J Mol Biol* 103(3):439–467.
2. Wray JS, Vibert PJ, Cohen C (1975) Diversity of cross-bridge configurations in invertebrate muscles. *Nature* 257(5527):561–564.

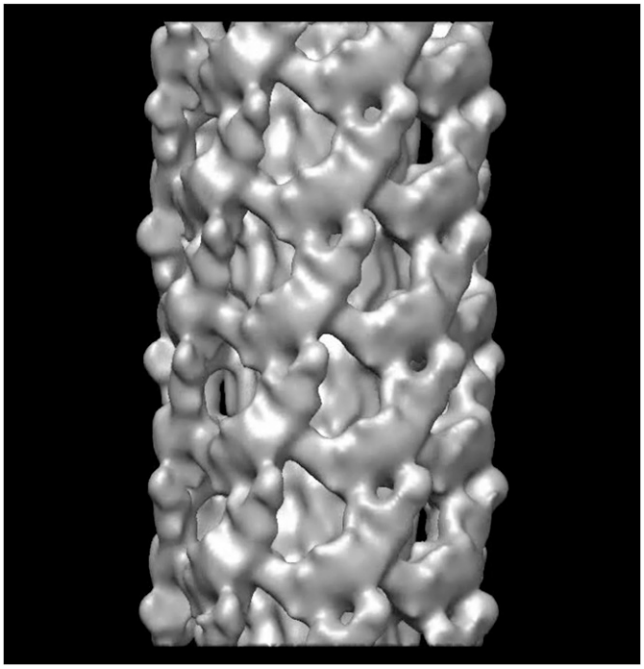

Movie S1. Three-dimensional reconstruction of scallop thick filament rotated about long axis. Reconstruction shows five 14.4-nm levels of sevenfold symmetric crowns of heads lying above the backbone, visible at lower radius (Fig. 2*A*). Five atomic models (ribbon and space-filling representations) have been fitted to show the intermolecular contacts (Fig. 3*A*). Bare zone direction is toward top.

Movie S1

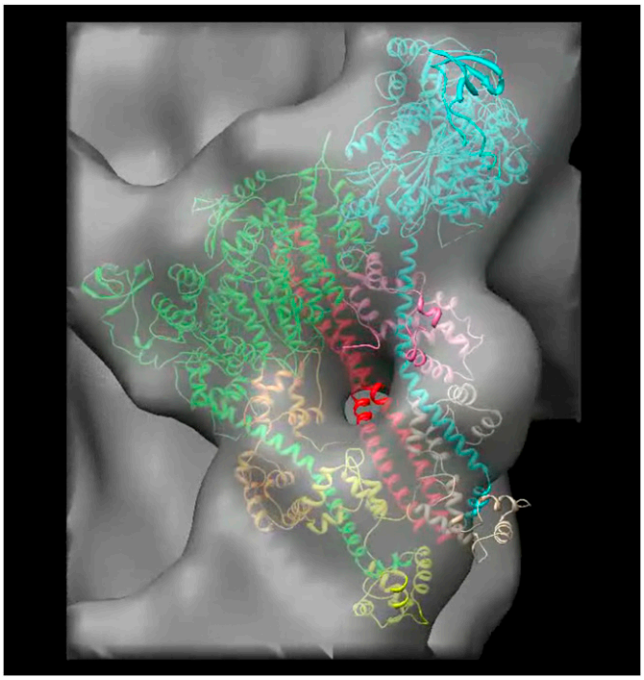

Movie S2. Fitting of ribbon and space-filling atomic models of scallop myosin head domains and S2 to one motif (Fig. 2*B*).

Movie S2

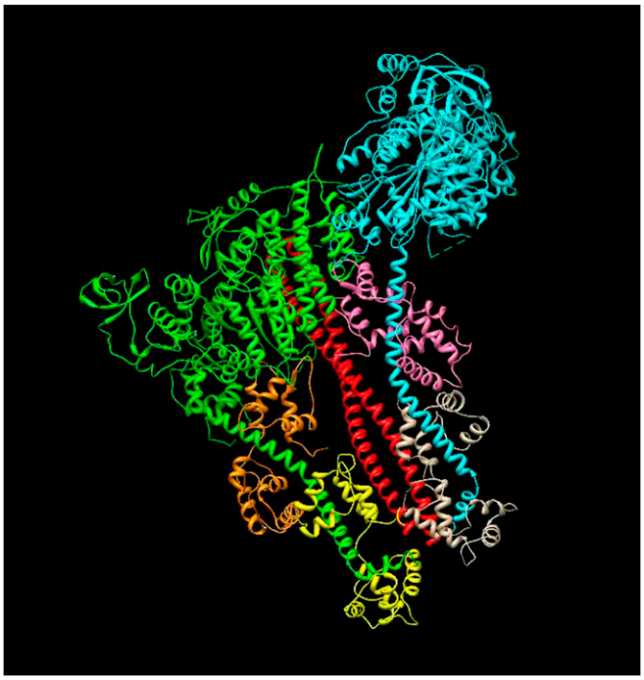

Movie S3. Atomic model of scallop head–head motif. The ribbon and space-filling models were produced by fitting crystallographic models for the scallop motor domain (PDB ID code 1QVI), regulatory domain (PDB ID code 3JTD), and N-terminal fragment of S2 (PDB ID code 3BAS) into the 3D reconstruction (Fig. 2*B*).

Movie S3

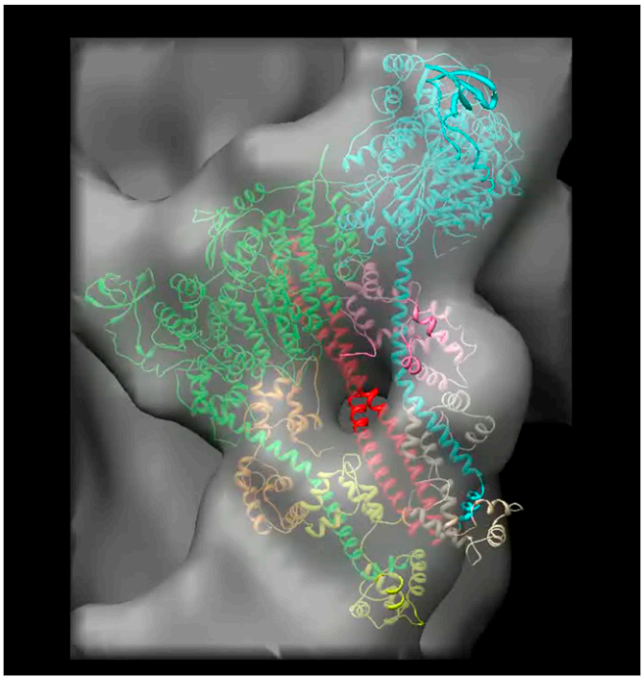

Movie S4. Fit of S2 (ribbon model) to the scallop head–head motif shown at different density contours. The "hole" in the density map between the regulatory domains is filled at lower contours to completely include all of the S2 in this region. The density "gap" between the head–head motif and the filament backbone (as viewed from the bare zone) is bridged at lower contours and shows the path S2 would eventually take to join with the subfilaments.

Movie S4